Surface Science 609 (2013) 177–182

Contents lists available at SciVerse ScienceDirect

Surface Science

journal homepage: www.elsevier.com/locate/susc

Alignment of benzene thin films on self-assembled monolayers by surface templating

Hanqiu Yuan, K.D. Gibson, Daniel R. Killelea [1], S.J. Sibener *

The James Franck Institute and Department of Chemistry, The University of Chicago, 929 East 57th Street, Chicago, IL 60637, USA

ARTICLE INFO

Article history:
Received 19 September 2012
Accepted 7 December 2012
Available online 19 December 2012

Keywords:
Self-assembled monolayers
Benzene adsorption
Surface templating
Vapor-phase deposition of molecules
Thin film epitaxy
Sticking and condensation

ABSTRACT

A key question in the epitaxial growth of materials is whether vapor-deposited molecules acquire an ordered structure that depends on the structure and chemical composition of the underlying substrate. In this paper we examine this question for metallic and chemically-tailored self-assembled monolayer (SAM) substrates, and show that proper selection of the templating substrate can lead to the deposition of nearly 100 layer thick molecular films that retain the alignment of the initial interface. In particular, we have examined benzene growth on gold, alkanethiol and phenoxy-terminated SAMs using a combination of in situ infrared spectroscopy and molecular beam techniques. When benzene molecules stick to a clean metal surface, the molecules in the first layer lie flat. However, after the deposition of a few layers, growth occurs as three-dimensional crystallites, resulting in randomly aligned polycrystalline domains. We found that there need not be an orientational transformation from the thin to thick structure for vapor-deposited molecules. Here, we vapor deposited benzene on phenoxy-terminated self-assembled monolayers (SAMs), and grew thick films of aligned benzene molecules. The alignment of the first layer of benzene molecules on the SAM was retained for more than 80 layers. In contrast, when methyl-terminated SAMs were used as a substrate, the thick film structure was indistinguishable from those with Au substrates.

1. Introduction

Organic semiconductors promise significant advantages in both the cost and performance of nanoscale devices over current silicon-based technologies [1]. In order to harness the rich functionality of organic molecules in devices such as light-emitting diodes [2] or field-effect transistors (FETs) [3,4], the interfacial properties between the underlying substrate and the organic materials must be controlled carefully to promote the formation of ordered domains [5,6]. One approach is to employ a well-ordered substrate surface with controlled structure and properties to template the growth of the organic film.

A particular template for the growth of molecular solids is a self-assembled monolayer (SAM) deposited on a metal surface. SAMs made from alkanethiols (R–SH) have found widespread applications in biotechnology, sensors, and surface passivation [7]. The interfacial structures of self-assembled monolayers prepared with normal alkanethiols and derivatives have been investigated for many years [8–11]. The structure of long alkanethiolate monolayers is known to be well ordered with the alkyl chains present in an all-trans conformation and canted off the surface normal by approximately 30°, presenting an ordered arrangement of the terminal groups at the surface [12–14]. What makes alkanethiolate SAMs such a versatile platform is that changing the terminal group of the alkanethiols will create an entirely new surface with its own functionality. Previous studies have shown the importance of the chemical composition of SAM terminal groups on influencing the structure formed by gas-phase deposition on solid surfaces. For example, Laskin and co-workers demonstrated the reactive landing of mass-selected biomolecules via covalent linking to the terminal groups of the SAM matrix, while retaining the secondary structure of the biomolecules [15]. Nakajima and coworkers have successfully used SAMs with different terminal groups to support gas-phase deposited transition metal-benzene sandwich complexes, where the physical integrity of the complexes remained intact, while the orientation and adsorption mechanisms varied by the functionality of the SAM terminal groups [16,17]. However, in these cases, large molecules were used and the delicate interplay between the molecule – molecule and molecule – surface interactions is washed out by the size of the molecules.

Non-covalent interactions between aromatic groups are known to impact a wide variety of phenomena in chemistry and biology [18], and a lot of effort has been dedicated to using aromatic or conjugated materials for the design of materials such as OFETs [19] in supramolecular chemistry [20] and for biological applications [21]. Among the various organic semiconductors investigated thus far, large aromatic polyacenes such as pentacene ($C_{22}H_{14}$) have garnered interest. These materials possess high charge carrier mobility in their crystalline phase and readily form highly ordered polycrystalline films, allowing the fabrication of high-performance thin-film OFET's [22]. Several research groups have

* Corresponding author.
E-mail address: s-sibener@uchicago.edu (S.J. Sibener).
[1] Present address: Department of Chemistry and Biochemistry, Loyola University Chicago, 1068W. Sheridan Rd., Chicago, IL 60660, USA.

0039-6028/$ – see front matter © 2012 Elsevier B.V. All rights reserved.
http://dx.doi.org/10.1016/j.susc.2012.12.005

reported surface-induced growth of ordered layers of these large molecules. On metal or silicon surfaces, pentacene molecules lie flat [23,24]. Often, the terminal groups of the SAM have little effect on the resultant structure of the film [25]. However, a perpendicular orientation relative to the substrate can significantly increase the charge transfer efficiency. Deposition of the desired perpendicular films has recently been obtained by using thiolate SAM buffer layers on Au(111) [26] as well as on Cu(100) [27] surfaces. Alteration of the grain morphology and microstructure of the pentacene film through slight variation of the interactions between pentacene and the SAM caused dramatic differences in OFET performance [28]. Although there are many examples demonstrating the aligning effects of SAMs, the basic physical principles governing organic thin film growth and how these principles relate to the substrate–molecule interactions are not well understood. Results from the study presented here focus on utilizing the fine balance between substrate–molecule interaction and intermolecular interactions to synthesize aligned molecular solids.

In this paper, we present our results for the ordered growth of a model organic precursor, benzene, as a function of the terminal functionalization of the SAM. The experiments were done in vacuum, using molecular beams to expose the surface to the benzene. We show that proper choice of the substrate facilitates the growth of ordered thin organic films. The structure of the terminal groups of the SAMs also has a significant influence on the dynamics of collisions between incoming species and the monolayer surface [29,30]. To demonstrate the strong effect of the substrate, we first characterized the surface structure of the SAMs, and then used a combination of molecular beam techniques to determine the sticking coefficient for benzene incident on a solid benzene surface and Fourier-transform reflection–absorption infrared spectroscopy (FT-IRRAS) to measure the alignment of the component benzene molecules in the organic layer. The growth of benzene films was studied on three different substrates. First, benzene film growth on bare gold surfaces was studied for comparison. The other two surfaces were made from SAMs with two different terminal groups, the first with methyl ($-CH_3$) termination (mSAM) and the second with a phenoxy terminal ($-O-C_6H_5$) group (pSAM), allowing direct comparison as to how the substrate–molecule interactions direct the subsequent growth of the molecular solid.

The IRRAS results clearly discriminate the different degrees of alignment of the benzene overlayers. We show that the benzene overlayer structure varies by substrate and evolves as the film thickens. At lower coverage, benzene in overlayers on pSAMs was highly tilted, while on bare Au, the benzene molecules lies flat. As the coverage was increased, the substrate-induced alignment diminished rapidly on both bare Au and mSAM, but the alignment was retained on pSAM. These results are the first report of such a persistent, and selective, templating of a solid structure in a molecular film from the underlying substrate in a vapor-deposition process.

Supersonic molecular beams provide an ideal tool to control the kinetic energy, incident angle, and exposure in order to influence the kinetics of growth of organic thin films [31]. In this study, we focus on the influence of the substrate surface properties on the adlayer structure, and a low energy beam was chosen. In the range of kinetic energies and incident angles used, no change was detected in the deposited benzene adlayer. In this study, the benzene beam falls into the energy regime where the benzene molecules adopt a combination of orientations with a slight preference in the edge-on mode [32,33]. However, the resulting film orientation was not affected by possible benzene partial alignment in the beam, as confirmed by the generation of the same film structures using either thermal or supersonic beam deposition.

2. Experimental

The experiments were conducted in specially built ultra-high vacuum molecular beam-surface scattering chambers. Previous publications [34,35] have described the apparatus in greater detail, so only a brief overview is presented here. The IRRAS analysis of SAMs and the in situ IRRAS analysis of benzene adlayer growth on different substrates were conducted in an ultra-high vacuum (UHV) chamber with a precision aligned molecular beam source. The sample was mounted on a five-axis manipulator and could be cooled below 120 K with liquid N_2. A PID controller (Eurotherm) controlled the heating of the sample, up to 600 K. A supersonic molecular beam of benzene (Sigma-Aldrich, 99.8%) was generated by bubbling helium or hydrogen through liquid benzene in a room-temperature bubbler, and expanded through a heatable nozzle ($T_n = 300–750$ K) with a 150 μm platinum orifice at a backing pressure of 100 psi.

The beam was characterized using time-of-flight techniques to determine the average energy of benzene in the beam and a liquid N_2 cooled quartz crystal microbalance (QCM) to measure the flux. One monolayer (ML) of benzene on gold is approximately 1.5×10^{14} molecules cm^{-2} [36], and the deposition rate of benzene from the beam on the 110 K QCM was (0.012 ± 0.003) ML s^{-1}. The peak kinetic energy of the beam was varied from 0.40 eV to 1.70 eV by adjusting the expansion temperature and carrier gas. For most experiments, the beam impinged at normal incidence; sticking probability measurements showed a decrease in the sticking probability at glancing incident angles (Θ_i) but no change in the structure of the benzene films on either Au or SAM surfaces were observed at different Θ_i. Benzene was also deposited on Au and SAM surfaces by backfilling the chamber with vapor ($p\approx1\times10^{-7}$ Torr) while the sample was held at 120 K.

The IRRAS spectra were obtained using a Nicolet model 6700 infrared spectrometer with a liquid nitrogen cooled MCT/A detector. The IR light was p-polarized and incident at a glancing angle of 75°. IRRAS spectra of the monolayers and benzene overlayers were collected at a resolution of 2 cm^{-1} and averaged over 500 scans. If not stated otherwise, the IRRAS spectra in this study were collected by the following procedure: (1) cool down of the substrate to the measurement temperature, (2) reference measurement, (3) benzene deposition and (4) sample measurement. The resultant difference spectra thus only show changes in the IR absorption, which includes the peaks due to benzene vibrations and the peaks corresponding to frequency and/or intensity changes of the SAM substrate. Some of the spectra presented have been base line corrected to facilitate the viewing of stacked plots; the corrections are in all cases minor.

Sticking probability (S) measurements were conducted in a separate UHV beam-surface scattering chamber. This apparatus is equipped with a Residual Gas Analyzer (RGA), and the sticking probability was determined using a modified King & Wells method [37] where the RGA signal with the cold surface (115 K) exposed to the beam is subtracted from the signal when the beam scatters from a warm surface where S is nearly zero. This method is well-suited for measuring small changes in S when S is nearly unity, as highlighted in a recent publication [34].

The SAM surfaces were prepared by immersing a cleaned poly-Au on mica substrate (Agilent Technologies Inc.) in a 1 mM solution of the thiol precursor at room temperature for at least 48 h. The SAMs were made from either 11-phenoxy 1-undecanethiol, $SH(CH_2)_{11}OC_6H_5$, (pSAM) or 1-hexadecanethiol, $CH_3(CH_2)_{15}SH$, (mSAM) (Asemblon Inc.). The average thickness of SAMs was measured at five different spots on each sample with a Gaertner L116S ellipsometer ($\lambda = 633$ nm, $n_{SAM} = 1.5$, $n_{Au} = 0.2246–3.5i$). The wettability of the SAM surfaces was determined by static contact angle measurements at ambient conditions. Microliter droplets of DI water were applied at the sample surface by a syringe infusion pump (Harvard Apparatus), and measurements of the contact angle were made on both sides of the two-dimensional projection of the droplet, captured by a video camera with a microscope lens. Each reported angle was averaged over five measurements on the same substrate sample.

3. Results and discussion

The key finding of this study is that phenyl-terminated self-assembled monolayers (p SAM) template the growth of aligned layers

of vapor deposited benzene molecules up to nearly 100 layers. In contrast, in the absence of a proper substrate template, the structure of the benzene film becomes insensitive to that of the substrate after a thickness of only 2 layers, as seen on methyl-terminated SAMs (mSAM) and polycrystalline gold substrates. IRRAS was used in situ to quantify the coverage and average tilt angle of the benzene molecules on these surfaces. We also determined the sticking coefficient for benzene on various surfaces and found that benzene sticking is highly probable on SAMs and benzene overlayers, and is invariant with respect to the structure of the benzene film. Moreover, the structures of the SAMs were determined, showing that the pSAM presents a hydrophobic, phenyl surface.

3.1. Structure and Interface of mSAM and pSAM

A clear characterization of the SAM structure, especially at the vacuum-solid interface, is crucial for the understanding of the subsequent benzene deposition. Characteristic IR modes in the C–H stretch region (2800–3000 cm^{-1}) of alkanethiolate SAMs in the IRRAS spectrum provide information about the ordering of the monolayer. The IRRAS spectra in Fig. 1 show the C–H stretch region (2700–3100 cm^{-1}) and the aromatic C–C stretch region (1400–1700 cm^{-1}) that clearly identify the two SAM surfaces. The mSAM IRRAS data (blue) are in good agreement with previous results [38,39], and the peak positions and widths of the C–H stretch peaks all indicate a densely packed, crystalline monolayer on the gold surface. The peaks at 2917 and 2848 cm^{-1} arise from the C–H stretch modes in the alkyl backbone and the two peaks at 2958 and 2873 cm^{-1} are from the terminal $-CH_3$ group. The IRRAS data for pSAM (red) show no terminal methyl features, and the alkyl backbone peaks are slightly blueshifted to 2923 and 2850 cm^{-1}, respectively, in excellent agreement with IR data in the literature [40]. Additionally, panel B in Fig. 1 shows the peaks characteristic of the terminal aromatic ring at 1608 and 1496 cm^{-1}. The relative intensities of these peaks are important for the determination of the orientation of the phenyl rings at the monolayer/vacuum interface. Due to the surface selection rule, only the projection of a mode normal to the surface will be observed with IRRAS. In the transmission IR spectrum of the 11-phenoxy undecanethiols, two modes at 1496 cm^{-1} and 1486 cm^{-1} are observed [40]. However, only the mode at 1496 cm^{-1} was observed in the IRRAS spectrum. These are both C–C stretches in the plane of the aromatic ring, but one is perpendicular to the surface (1496 cm^{-1}), and the other is apparently parallel (1486 cm^{-1}), since only one is seen in the IRRAS spectrum. The surface selection rule suggests that the aromatic ring has its C_1-C_4 axis perpendicular to the surface. In addition, a small spectroscopic feature attributed to an aromatic C–H stretching mode (near 3066 cm^{-1}) was observed in the transmission spectrum yet absent in the IRRAS spectrum [40], indicating that inclusion of the ether linkage does not allow for edge-to-face interactions of the terminal phenyl rings. The strong intensity of the peaks at 1608 and 1496 cm^{-1} indicates that the phenyl rings are largely perpendicular to the substrate surface.

The intensities of the alkyl backbone C–H stretching modes for pSAM are close to the values of normal alkanethiolate SAMs, like mSAM, indicating a similar chain tilt angle [12,41]. The asymmetric and symmetric CH_2 vibrational modes were found at 2923 and 2850 cm^{-1}, respectively, and their widths were characteristic of a well-ordered monolayer. Also, the thickness of the two SAMs determined from ellipsometry (19.2 ± 2 Å) closely resembled that of the calculated value if a tilt angle of 30° is assumed (~19 Å), or the thickness of the phenyl SAM without the ether linkage (18.5 ± 1.4 Å) [40]. In summary, the IRRAS data shows that the phenyl rings of the prepared pSAM are largely perpendicular to the substrate surface, thus shielding the phenoxy oxygen from exposure at the vacuum-solid interface. Furthermore, the average tilt angle of the alkyl chains is similar to the unsubstituted counterparts. Finally, the wettability of these surfaces provides further evidence about the surface structure of the SAMs. The contact angle of water on the bare gold is <5° and on mSAM is 110 ± 1°. The small contact angle for water on the bare gold surface means the surface is nearly completely wetted. On the other hand, the large contact angle reveals the hydrophobic nature of mSAM, in good agreement with literature values for the same system [42]. The contact angle of water on pSAM was 93 ± 2°, showing a hydrophobic surface where the terminal phenyl ring obscures the O in the SAM, strongly suggesting that the surface is composed of vertical phenyl rings.

3.2. Sticking of benzene on SAM surfaces

When gas-phase benzene molecules strike a metal surface, they can either stick or scatter from the surface back into the gas phase. On a SAM, the situation is slightly more complicated, for the benzene molecules could not only scatter or stick to the topmost layer of the surface, but they could possibly penetrate into the SAM alkyl chain matrix, or even penetrate deep enough to stick to the gold substrate itself. Methyl-terminated SAMs have been shown to efficiently dissipate excess kinetic energy of projectiles [29], and thus sticking is highly probable. Because the benzene molecules are hitting the surface with an appreciable amount of energy, up to 2.5 eV, it is possible that partial disordering and localized melting of the monolayer could take place. However, we found that both mSAM and pSAM were very stable during all benzene depositions and saw no evidence of any disruption or desorption of the alkyl backbones of the SAMs themselves, as the peak intensities and shapes were unchanged throughout the exposure [43]. These results mean that benzene sticking to the SAM surfaces, and subsequently to benzene covered surfaces, was the only significant

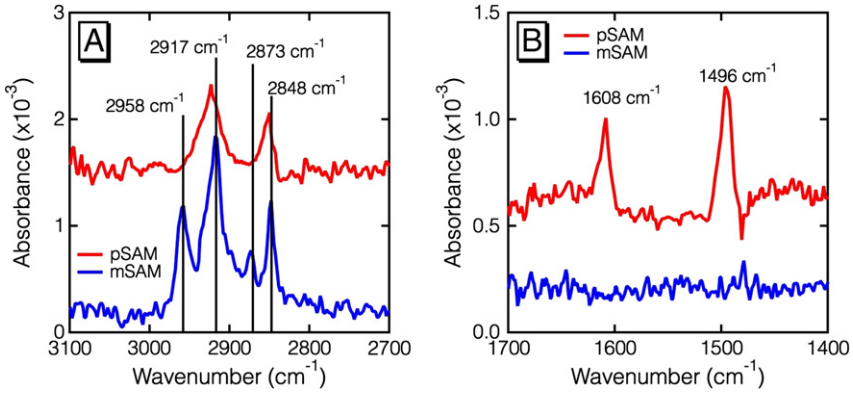

Fig. 1. IRRAS spectra of methyl-terminated SAM (mSAM, blue) and phenoxy-terminated SAM (pSAM, red) on polycrystalline gold at a surface temperature (T_s) of 120 K. The C–H stretch region is shown in panel A) and the C–C ring stretch region between 1700 and 1400 cm^{-1} is shown in B). The two peaks at 2915 and 2848 cm^{-1} are assigned to the $-CH_2-$ backbone present for both SAMs, and the unique features are peaks at 2958 and 2873 cm^{-1} from the terminal $-CH_3$ group on the mSAM, and the phenyl ring stretch peaks at 1608 and 1496 cm^{-1} on the pSAM.

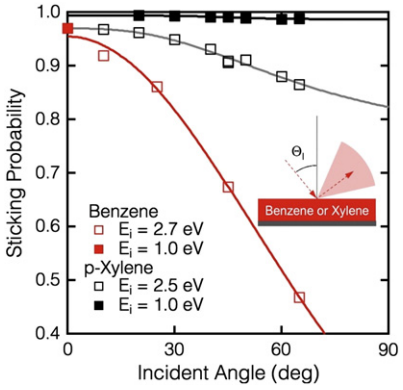

Fig. 2. Sticking coefficient of benzene on benzene covered Rh(111) (red) and p-xylene on p-xylene on Rh(111) (black) as a function of incident angle.

uptake channel of any importance at these incident energies and surface temperatures.

It was important to first establish the sticking probability of benzene on a benzene-covered surface to properly interpret the IRRAS data. If the sticking coefficient were coverage-dependent, the deposition rate would have varied, and could have altered the structure of the film. As reported in a previous publication [34], our IRRAS system provides a relative sticking coefficient by monitoring the rate of film growth, and uses a separate system to determine the absolute sticking coefficient with the modified King & Wells technique in the differentially pumped beam-surface scattering chamber. As shown in Fig. 2, the sticking probability of benzene on a benzene-covered surface is very close to unity. For benzene with 1.0 eV initial translational energy (E_I) at normal incidence, S = 0.977, and is slightly lower for benzene with E_I = 2.5 eV. Once the metal was completely covered by benzene, the sticking coefficient was constant for all coverages, and the sticking coefficient decreased as the incident angle became more glancing. This is similar to previous results for water on ice surfaces; because of good momentum matching, sticking is highly probable [44]. It is noteworthy to compare the sticking for benzene to p-xylene. Xylene is slightly more massive than benzene and due to the *para* methyl substitution on the phenyl ring, is elongated compared to benzene molecules. As a result, sticking was even more probable for p-xylene at all incident angles. In the case of p-xylene, parallel momentum was not stringently conserved. For most of the experimental data presented here, the benzene was landing on a benzene-coated surface at normal incidence where the sticking coefficient was invariant.

3.3. IRRAS measurement of benzene alignment

Benzene adsorption on many active metal surfaces is fairly well characterized [36,45–49]. However, there are fewer experimental [50,51] and theoretical [52,53] reports concerning benzene adsorption on gold surfaces. Understanding the structure of benzene on the metal surface is crucial for a thorough understanding of the more complicated substrate–adsorbate and adsorbate–adsorbate interactions in thin films. In the present study, we first investigated benzene adlayer growth on Au, providing a basis for comparison to the benzene adsorption on Au modified with SAMs.

IRRAS spectra of several coverages (1 ML, 2 ML, and 4 ML) of benzene adsorbed on gold are shown in Figs. 3 and 4 (80 ML) by black lines. Three separate portions of the spectrum are shown, the ν_{19} in-plane aromatic C–C stretch between 1500 and 1450 cm^{-1} (A), the ν_{18} in-plane C–H bend between 1075 and 1000 cm^{-1} (B) and the ν_{11} out-of-plane C–H bend between 750 and 650 cm^{-1} (C). The above modes are the most structure sensitive and provide essential information about the benzene adlayer structure. The data in Fig. 3 show how the absorption features of the films evolve with coverage (1, 2, and 4 ML) and are in good agreement to previous studies of benzene adsorption on transition metal surfaces [48,51]. On single-crystalline metal surfaces planar aromatic hydrocarbons such as benzene form a layer of closely packed, flat-lying molecules [45,47–49]. As the benzene film thickens, the intermolecular interactions between benzene molecules dominate and multilayer benzene films have a bulk crystalline "herringbone" structure due to benzene–benzene face-to-edge interaction. IRRAS is able to determine the bulk crystalline structure and the average tilt angle of the benzene molecules with respect to the gold surface plane. Spectroscopic information on the average benzene orientation of the adlayers on different substrates has been derived from high resolution electron energy loss spectroscopy (HREELS) [36,54] and IRRAS [55]. IRRAS has very high spectral resolutions at frequencies above 600 cm^{-1}. Moreover, due to the restriction of the surface selection rule [56,57], only vibrational modes with dipole moments perpendicular to the surface are observable in the IRRAS spectrum, allowing semi-quantitative determination of molecular orientations and in situ monitoring of benzene adlayer growth.

At monolayer and lower coverages (1 ML traces), only the ν_{11} mode at 682 cm^{-1} was observed. Significant changes occur in the IR spectra

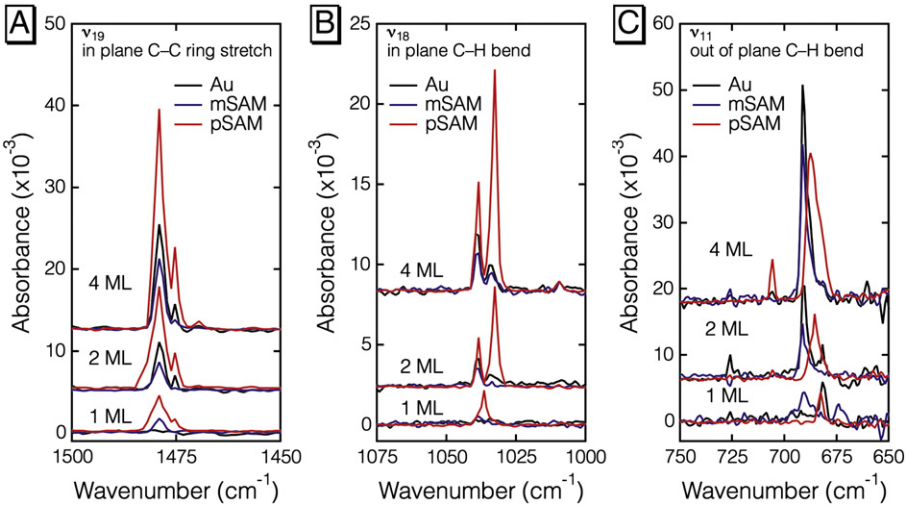

Fig. 3. Details of IRRAS spectra of benzene films on Au (black), mSAM (blue), and pSAM (red) at coverages of 1, 2, and 4 ML. The differences in the absorption features are evident at low coverage and the unique features of the film on pSAM seen at the second layer persist to 80 ML as shown in Fig. 4.

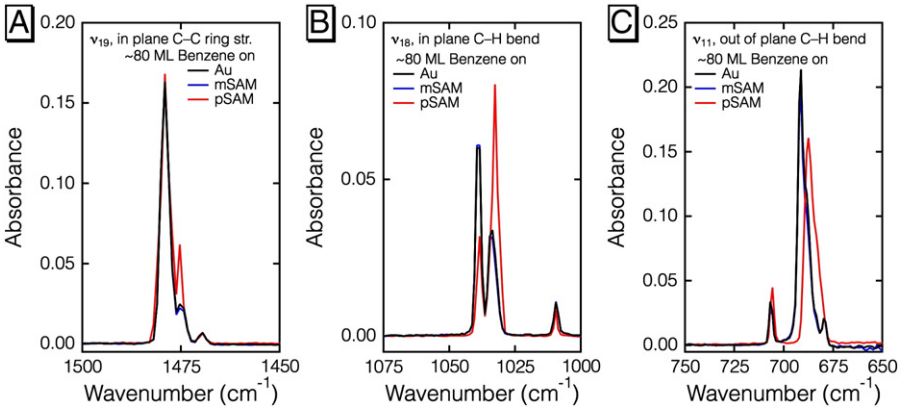

Fig. 4. IRRAS spectra of about 80 ML of benzene on three different surfaces, Au (black), mSAM (blue), and pSAM (red) at $T_s = 120$ K. Benzene films grown on pSAM are distinguished from the same film grown on either mSAM or Au by peak shifts to 1475 cm^{-1}, 1038 cm^{-1}, 1032 cm^{-1}, and 688 cm^{-1}.

at higher coverages. First, the ν_{18} and ν_{19} peaks appear in the spectra at 1038 and 1479 cm^{-1} respectively, and they show peak splitting characteristic of crystalline benzene even at coverages as low as 2 ML. Second, a new peak near the ν_{11} peak grows in at 690 cm^{-1}. This peak indicates the formation of 3-D crystallites, and is consistent with previous studies [55] that showed that once the first layer is filled, benzene film growth quickly diverges from the layer-by-layer mechanism. However, there is a mismatch between the flat-lying, parallel configuration and the characteristic face-on-edge herringbone arrangement adopted in the bulk crystalline benzene. It is possible that this strain was released by the formation of crystallites above a critical size [55] and the limiting factor of this transition was the minimum size required for crystalline benzene to be more stable [55]. Thus, upon further dosing, the benzene adlayer transitioned to a bulk crystalline phase. The spectra also suggest a more or less homogenous crystalline adlayer on the gold surface. The average tilt angle of the benzene increased and remained stable of near 45°, as shown in Fig. 5.

The average orientation of the benzene molecules in thin films on gold surfaces is determined from the IRRAS spectra and knowledge of the structure of benzene. In the IRRAS spectrum of benzene, the vibrational modes with A_{2u} (i.e. ν_{11}) symmetry give rise to transition dipoles perpendicular to the benzene ring plane. In contrast, the modes with E_{1u} (i.e. ν_{18} and ν_{19}) symmetry arise from dipoles oriented parallel to the benzene ring plane. Therefore, the orientation of the molecules with respect to the substrate surface is determined by directly comparing the A_{2u} and E_{1u} modes, i.e. the out-of-plane and in-plane C–H bending modes of benzene, as shown in Eq. (1) [58,59]. The resulting tilt angle is the average angle between the benzene ring plane and the substrate surface plane.

$$\tan^2\theta = \left(\frac{\mu_{A_{2u}}}{\mu_{E_{1u}}}\right)^2 \frac{\nu_{A_{2u}}}{\nu_{E_{1u}}} \frac{A_{E_{1u}}}{A_{A_{2u}}}. \quad (1)$$

In the equation, μ is the transition dipole moment, ν is the resonant frequency, and A is the integrated area of the absorption peak.

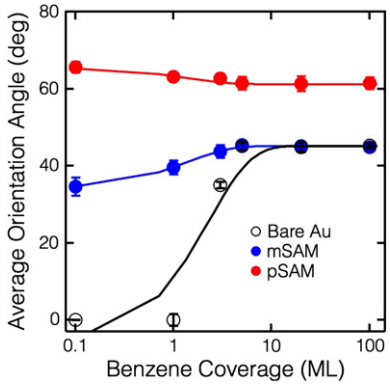

Fig. 5. The calculated average tilt angle as a function of benzene coverage. After about 2 ML of benzene is deposited, the tilt angle reaches a steady value characteristic of the underlying substrate, ≈45° on Au or mSAM suggesting a stochastic arrangement, or 60° on pSAM which is indicative of a more aligned solid structure.

3.4. Templated growth of aligned benzene adlayers

Comparison of the IRRAS spectra of benzene overlayers on mSAM and gold shows that the adlayer spectra differ at low (<2 ML) coverages, but as the films become thicker, these differences vanish and their spectra become indistinguishable. However, this is not true with the pSAM surface. Instead, the initial spectral differences persist to almost 100 layers thickness, as shown in Fig. 4. The pSAM surface templates an aligned film whereas the mSAM or gold does not.

At sub-monolayer coverages, the most distinctive difference of the benzene IR spectrum on mSAM is that the in-plane modes appear, while the out-of-plane peak's width and frequency (684 cm^{-1}) corresponding to a disordered phase. Above monolayer coverage, the crystalline phase peak in the out-of-plane mode (690 cm^{-1}) shows up, indicating the formation of 3-D crystallites. At multilayer coverages, the IR spectra are essentially the same to those of benzene on gold: crystalline with the same average tilt angle.

As discussed previously, the benzene ring lies flat on the Au substrate at sub-monolayer coverage. With the addition of an alkanethiolate monolayer, the Au-benzene distance increases, and the interaction therefore decreases. Due to the weak interaction between the methyl terminal groups on mSAM surface and the benzene molecules (π-sp^3), the adsorbed benzene lacks a preferred geometry of alignment but appears to be tilted from the substrate surface plane. The disorder indicated by the peak shift and increased width of the out-of-plane C–H stretch (ν_{11}) is probably due to inhomogeneous broadening due to the amorphous nature of the adsorption. At higher coverages, the benzene becomes crystalline. Unlike in the sub-monolayer regime, once the substrate is covered, the growth of the benzene film in the multilayer regime appears remarkably similar to growth on Au.

As shown in Figs. 3 and 4, benzene overlayer growth on pSAM shows significant, and interesting, differences from that on mSAM or gold. The surface of the pSAM is composed of phenyl rings that are almost perpendicular to the metal substrate, and this surface structure templates the orientation of the first and the subsequent benzene adlayer orientation. On all three substrates, the benzene molecules in the multilayer are tilted from the surface normal, as evidenced by the

appearance of both in-plane and out-of-plane modes. However, the IRRAS spectra at the same surface coverage differ strikingly in the relative intensities of the in- and out-of-plane peaks for the pSAM versus the other two substrates. The out-of-plane peak (ν_{11}) is much weaker compared to the in-plane peaks on pSAM, while the same peak on the mSAM is essentially the same to that on bare Au, especially at high coverage. This difference indicates that the benzene molecules deposited on pSAM on average adopt a different orientation from that on Au or on mSAM. The average tilt angle of the benzene molecules on the pSAM was found to be about 60° for all coverages investigated at 120 K. Fig. 5 plots the average tilt angle at various benzene coverages on pSAM (red), mSAM (blue), and gold (black) and shows the rapid convergence of films on gold and mSAM and the persistent difference of the film grown on pSAM. The primary distinction between benzene films grown on pSAM from Au or on mSAM was that the benzene film on pSAM shows very strong in-plane modes at all coverages, which means that the molecules are aligned so that the intensity of the out-of-plane modes are weakened by the surface selection rule. On the other hand, the relative intensity of the in-plane and out-of-plane modes are essentially the same in multilayer benzene films on mSAM and gold, meaning that there is no alignment effect on the molecules in thick films from these two substrates.

The alignment of benzene molecules in films grown on pSAM is thermally stable. When heated, the benzene adlayer desorbs before any changes were seen in the IRRAS spectra. Annealing the films at 140 K yielded only minor increases (~1–2°) in the tilt angle. Moreover, the benzene orientation was the same for deposition at higher surface temperatures, up to about 155 K where the sticking coefficient was less than the desorption rate.

It is interesting to note that the energy of the incident benzene molecules had no apparent effect on the resultant structure of the benzene film. For all three surfaces studied, gold, mSAM, and pSAM, the film alignment was invariant whether the benzene was deposited with the molecular beam or by backfilling the chamber. The collision energies are very different for these two cases. When the surface is dosed with a molecular beam the incident energy of the molecules is a narrow distribution around an average E_I between 0.4 and 2.7 eV. When the chamber is backfilled, typically to 1×10^{-7} Torr, the molecules are incident in a cosine distribution of Θ_I with an $E_I = 13$ meV. In addition, there appeared to be no change in sticking on benzene-covered metal or SAM surfaces with E_I. It seems that any excess energy is readily accommodated by the surface and neither damages the molecular lattice nor crystallizes the unaligned films on mSAM or Au.

4. Conclusion

We have shown that the alignment of vapor-deposited thin organic molecular films is possible by proper selection of the growth substrate. When benzene molecules are deposited on phenoxy-terminated self-assembled monolayers at 120 K, an aligned film grows where the average orientation of the benzene molecules is 60° off the substrate surface. This alignment is present in the first benzene layer on the SAM and is maintained to a thickness of nearly 100 layers. This is in marked contrast to benzene films grown on either bare gold or methyl-terminated SAMs, where there may be a unique first layer, but the film quickly becomes a polycrystalline solid with a stochastic arrangement of the crystallites. These results show that proper choice of the substrate has profound impact on the structure of the deposited film. Most importantly, careful balancing of the intermolecular forces and the interactions with the substrate allows for the creation of unique structures from materials that normally do not exhibit such correlated structural properties.

Acknowledgments

This work was supported by the NSF, Award No. CHE-0911424, with additional infrastructure support coming from the central facilities of the Materials Research Science and Engineering Center at The University of Chicago, NSF-DMR-0213745. We also gratefully acknowledge DTRA, Grant No. HDTRA1-11-1-0001, for generous support of the trace detection components of this study.

References

[1] S.R. Forrest, Chem. Rev. 97 (1997) 1793.
[2] A. Dodabalapur, Solid State Commun. 102 (1997) 259.
[3] G. Horowitz, Adv. Mater. 10 (1998) 365.
[4] H.E. Katz, A.J. Lovinger, J. Johnson, C. Kloc, T. Siegrist, W. Li, Y.Y. Lin, A. Dodabalapur, Nature 404 (2000) 478.
[5] C.D. Dimitrakopoulos, S. Purushothaman, J. Kymissis, A. Callegari, J.M. Shaw, Science 283 (1999) 822.
[6] I.G. Hill, D. Milliron, J. Schwartz, A. Kahn, Appl. Surf. Sci. 166 (2000) 354.
[7] C. Vericat, M.E. Vela, R.C. Salvarezza, PCCP 7 (2005) 3258.
[8] R.G. Nuzzo, D.L. Allara, J. Am. Chem. Soc. 105 (1983) 4481.
[9] D.L. Allara, R.G. Nuzzo, Langmuir 1 (1985) 45.
[10] D.L. Allara, R.G. Nuzzo, Langmuir 1 (1985) 52.
[11] J.D. Swalen, D.L. Allara, J.D. Andrade, E.A. Chandross, S. Garoff, J. Israelachvili, T.J. Mccarthy, R. Murray, R.F. Pease, J.F. Rabolt, K.J. Wynne, H. Yu, Langmuir 3 (1987) 932.
[12] C.D. Bain, E.B. Troughton, Y.T. Tao, J. Evall, G.M. Whitesides, R.G. Nuzzo, J. Am. Chem. Soc. 111 (1989) 321.
[13] A. Ulman, J.E. Eilers, N. Tillman, Langmuir 5 (1989) 1147.
[14] C.E.D. Chidsey, D.N. Loiacono, Langmuir 6 (1990) 682.
[15] J. Laskin, P. Wang, O. Hadjar, J. Am. Chem. Soc. 129 (2007) 8682.
[16] A. Nakajima, K. Ikemoto, S. Nagaoka, T. Matsumoto, M. Mitsui, J. Phys. Chem. C 113 (2009) 4476.
[17] A. Nakajima, S. Nagaoka, K. Ikemoto, T. Matsumoto, M. Mitsui, J. Phys. Chem. C 112 (2008) 6891.
[18] C.A. Hunter, Chem. Soc. Rev. 23 (1994) 101.
[19] J.E. Anthony, Angew. Chem. Int. Ed. 47 (2008) 452.
[20] Y.Z. Wang, A.X. Wu, Chin. J. Org. Chem. 28 (2008) 997.
[21] B.M. O'Neill, J.E. Ratto, K.L. Good, D.C. Tahmassebi, S.A. Helquist, J.C. Morales, E.T. Kool, J. Org. Chem. 67 (2002) 5869.
[22] H. Klauk, M. Halik, U. Zschieschang, G. Schmid, W. Radlik, W. Weber, J. Appl. Phys. 92 (2002) 5259.
[23] F.-J. Meyer zu Heringdorf, M.C. Reuter, R.M. Tromp, Nature 412 (2001) 517.
[24] C.B. France, P.G. Schroeder, J.C. Forsythe, B.A. Parkinson, Langmuir 19 (2003) 1274.
[25] D. Kafer, L. Ruppel, G. Witte, Phys. Rev. B 75 (2007).
[26] W.S. Hu, Y.T. Tao, Y.J. Hsu, D.H. Wei, Y.S. Wu, Langmuir 21 (2005) 2260.
[27] A. Kanjilal, F. Bussolotti, F. Crispoldi, M. Beccari, V. Di Castro, M.G. Betti, C. Mariani, J. Phys. IV 132 (2006) 301.
[28] J.R. Engstrom, T.V. Desai, A.R. Woll, F. Sehreiber, J. Phys. Chem. C 114 (2010) 20120.
[29] B.S. Day, S.F. Shuler, A. Ducre, J.R. Morris, J. Chem. Phys. 119 (2003) 8084.
[30] M.K. Ferguson, J.R. Lohr, B.S. Day, J.R. Morris, Phys. Rev. Lett. 92 (2004).
[31] A.S. Killampalli, T.W. Schroeder, J.R. Engstrom, Appl. Phys. Lett. 87 (2005).
[32] F. Pirani, M. Bartolomei, V. Aquilanti, M. Scotoni, M. Vescovi, D. Ascenzi, D. Bassi, D. Cappelletti, J. Chem. Phys. 119 (2003) 265.
[33] F. Pirani, D. Cappelletti, M. Bartolomei, V. Aquilanti, M. Scotoni, M. Vescovi, D. Ascenzi, D. Bassi, Phys. Rev. Lett. 86 (2001) 5035.
[34] K.D. Gibson, D.R. Killelea, H.Q. Yuan, J.S. Becker, S.J. Sibener, J. Chem. Phys. 134 (2011).
[35] H.Q. Yuan, D.R. Killelea, S. Tepavcevic, S.I. Kelber, S.J. Sibener, J. Phys. Chem. A 115 (2011) 3736.
[36] M. Xi, M.X. Yang, S.K. Jo, B.E. Bent, P. Stevens, J. Chem. Phys. 101 (1994) 9122.
[37] D.A. King, M.G. Wells, Surf. Sci. 29 (1972) 454.
[38] M.D. Porter, T.B. Bright, D.L. Allara, C.E.D. Chidsey, J. Am. Chem. Soc. 109 (1987) 3559.
[39] K.R. Rodriguez, S. Shah, S.M. Williams, S. Teeters-Kennedy, J.V. Coe, J. Chem. Phys. 121 (2004) 8671.
[40] F. Cavadas, M.R. Anderson, J. Colloid Interface Sci. 274 (2004) 365.
[41] Y.Y. Luk, N.L. Abbott, J.N. Crain, F.J. Himpsel, J. Chem. Phys. 120 (2004) 10792.
[42] L.H. Dubois, B.R. Zegarski, R.G. Nuzzo, J. Am. Chem. Soc. 112 (1990) 570.
[43] S. Nagaoka, K. Ikemoto, T. Matsumoto, M. Mitsui, A. Nakajima, J. Phys. Chem. C 112 (2008) 15824.
[44] D.R. Killelea, K.D. Gibson, H. Yuan, J.S. Becker, S.J. Sibener, J. Chem. Phys. 136 (2012).
[45] M.X. Yang, M. Xi, H.J. Yuan, B.E. Bent, P. Stevens, J.M. White, Surf. Sci. 341 (1995) 9.
[46] F.P. Netzer, Langmuir 7 (1991) 2544.
[47] P. Yannoulis, R. Dudde, K.H. Frank, E.E. Koch, Surf. Sci. 189 (1987) 519.
[48] S. Haq, D.A. King, J. Phys. Chem. 100 (1996) 16957.
[49] J.H. Kang, R.L. Toomes, J. Robinson, D.P. Woodruff, O. Schaff, R. Terborg, R. Lindsay, P. Baumgartel, A.M. Bradshaw, Surf. Sci. 448 (2000) 23.
[50] S.M. Wetterer, D.J. Lavrich, T. Cummings, S.L. Bernasek, G. Scoles, J. Phys. Chem. B 102 (1998) 9266.
[51] D. Syomin, J. Kim, B.E. Koel, G.B. Ellison, J. Phys. Chem. B 105 (2001) 8387.
[52] E. Abad, Y.J. Dappe, J.I. Martinez, F. Flores, J. Ortega, J. Chem. Phys. 134 (2011).
[53] E. Abad, J. Ortega, Y. Dappe, F. Flores, Appl. Phys. A: Mater. Sci. Process. 95 (2009) 119.
[54] P. Jakob, D. Menzel, Surf. Sci. 220 (1989) 70.
[55] P. Jakob, D. Menzel, J. Chem. Phys. 105 (1996) 3838.
[56] R.G. Greenler, J. Chem. Phys. 44 (1966) 310.
[57] R.G. Greenler, J. Chem. Phys. 50 (1969) 1963.
[58] J.F. Fan, M. Trenary, Langmuir 10 (1994) 3649.
[59] M. Trenary, Annu. Rev. Phys. Chem. 51 (2000) 381.